Science of the Total Environment 773 (2021) 144818

Contents lists available at ScienceDirect

Science of the Total Environment

journal homepage: www.elsevier.com/locate/scitotenv

Aircraft-based observation of gaseous pollutants in the lower troposphere over the Beijing-Tianjin-Hebei region

Ruojie Zhao [a], Baohui Yin [a], Nan Zhang [a], Jing Wang [a], Chunmei Geng [a,*], Xinhua Wang [a], Bin Han [a], Kangwei Li [a], Peng Li [b], Hao Yu [a], Wen Yang [a,*], Zhipeng Bai [a]

[a] State Key Laboratory of Environmental Criteria and Risk Assessment, Chinese Research Academy of Environmental Sciences, Beijing 100012, PR China
[b] Tianjin Eco-Environmental Monitoring Center, Tianjin 300191, PR China

HIGHLIGHTS

- Aircraft-based measurements were conducted over the Beijing-Tianjin-Hebei region.
- First simultaneous observations of tethered balloon and aircraft were analyzed.
- Planetary boundary layer significantly suppressed the vertical exchange.
- Southerly air masses resulted in the high concentrations of gaseous pollutants.

GRAPHICAL ABSTRACT

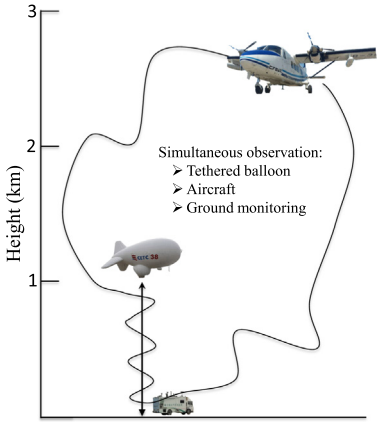

ARTICLE INFO

Article history:
Received 1 July 2020
Received in revised form 25 September 2020
Accepted 23 December 2020
Available online 27 January 2021

Editor: Jianmin Chen

Keywords:
Beijing-Tianjin-Hebei (BTH) region
Aircraft measurement
Gaseous pollutants
Vertical distribution

ABSTRACT

To investigate the spatial and vertical distribution of atmospheric pollutants (SO_2, NO_x, CO and O_3), aircraft-based measurements (model: Yun-12, 12 flights, 27 h total flight time) were conducted from near the surface up to 2400 m over the Beijing-Tianjin-Hebei (BTH) region between June 17th and July 22nd 2016. The results showed that high concentrations of primary gaseous pollutants (SO_2, NO_x, CO) were generally present in Beijing, Tianjin, Langfang and Tangshan areas, while high values of O_3 frequently appeared in areas far from the city. The flights at noon and dusk measured higher O_3 concentrations at 600 m and lower O_3 concentrations at higher altitudes, implying a strong influence by photochemical production. Back trajectory analysis suggested that the high levels of gaseous pollutants, especially at 600 m, were associated with pollution sources transported from the southerly direction during the observation period. The first simultaneous vertical distribution measurements using aircraft and tethered balloon were conducted in Gaocun (a rural site between Beijing and Tianjin) on June 17th. The results indicated that an inversion layer at the top of the planetary boundary layer (PBL) significantly suppressed vertical exchange through the PBL and resulted in a "two-layer" vertical distribution of pollutants above and below the PBL. Additionally, a residual high O_3 layer (79.9 ± 2.5 ppb, 500–1000 m) was observed above the PBL, and it contributed to the surface peak O_3 level at noon through downward transport along with the opening up of the PBL. These results indicate that coupled effects of horizontal and vertical transport should be investigated in future studies to improve the chemical transport models used to study the vertical distribution and regional transport over the BTH region.

* Corresponding authors.
E-mail addresses: gengcm@craes.org.cn (C. Geng), yangwen@craes.org.cn (W. Yang).

https://doi.org/10.1016/j.scitotenv.2020.144818
0048-9697/

1. Introduction

In recent years, air pollution has become one of the most serious and concerned environmental problems in China. The BTH (Beijing-Tianjin-Hebei) region was the one of the severely air polluted across the world (Li et al., 2017a; Song et al., 2017; Han et al., 2016). More than five of the annual top ten cities with relatively poor air quality, locate in Hebei province from 2013 to 2018 (http://www.mee.gov.cn/hjzl/zghjzkgb/lnzghjzkgb/). A number of researchers conducted a series of studies, which systematically expounded the characteristics of and changes to air quality (Xu et al., 2019; Tian et al., 2019; He et al., 2017), the relationship between meteorological conditions and air pollution (He et al., 2018; Zhang et al., 2012; He et al., 2017; Shi et al., 2018), mutual inter-city and regional transport contributions (Cheng et al., 2018; Chang et al., 2019). These previous studies were mainly based on routine ground monitoring. Actually, the intense turbulence can result in significant vertical and horizontal mixing in the lower troposphere and the regional vertical distributions of the air pollutants can provide more accurate information on the impact of short- or long-range transport and the boundary layer change. Therefore, the observation only based on the ground monitoring shows a great limitation and it is necessary to perform regional vertical monitoring of the air pollutants within the lower troposphere.

At present, four direct measuring methods have been used to conduct vertical observations: 1) unmanned aerial vehicles (UAV, Villa et al., 2016; Peng et al., 2015; Li et al., 2018; Li et al., 2017b); 2) towers (Meng et al., 2008; Aneja et al., 2000; Sun et al., 2013; Zhang et al., 2011); 3) tethered balloons (Zhang et al., 2019; Zhang et al., 2017; Li et al., 2015; Sangiorgi et al., 2011; Greenberg et al., 2009); and 4) aircraft (Chen et al., 2013; Ding et al., 2008; Ma et al., 2012; Zhang et al., 2014). Among these methods, aircraft measurement has the advantage on covering larger spatial and vertical variations of air pollutants due to their relatively high capacity and ability to be deployed to many areas of interest within a short time. Aircraft enables mobile synchronous vertical and horizontal observations, which can provide data relating to the boundary layer effect, regional transport, and distribution and dynamics in the lower atmosphere (Taubman et al., 2006).

The earliest aircraft-based observations in China were conducted since 1958 to study the weather modification (You and Liu, 1995, Quan and Jia, 2020). Several aircraft observation programs have also been carried out over the BTH region. The Influence of Pollution on Aerosols and Cloud Microphysics in North China (IPAC-NC) program in spring 2006 found widespread haze clouds with high levels of air pollutants and particles, and elucidated the role of the oxidation pool in the Huabei region (Ma et al., 2012; Ma et al., 2010). The global Measurement of Ozone and Water Vapor by Airbus In-Service Aircraft (MOZAIC) project, recorded the O_3 profiles from 1995 to 2005 and identified increasing photochemical pollution over Beijing and the North China Plain (NCP, Ding et al., 2008). The Campaigns of Air Quality Research in Beijing and Surrounding Regions in 2008 (CAREBeijing-2008) investigated the air pollution characteristics during and after the Beijing Olympics and suggested four distinct sources of air pollutants (Zhang et al., 2014). The vertical and horizontal O_3 distributions measured from 159 flights from 2007 to 2010 over Beijing and its surrounding areas indicated a transition altitude (~1 km) of ozone formation and an enhanced impact of city plumes on O_3 levels in downwind areas (Chen et al., 2013). Other aircraft measurements have also recorded an elevated pollution layer (EPL) in Beijing or the NCP, which was attributed to the Mountain Chimney Effect caused by mountain-valley breezes (Chen et al., 2009) or the lifting of pollutants by anticyclone circulation and surrounding terrain (Liu et al., 2018). To our knowledge, most previous aircraft-based measurement studies over the BTH region were conducted before 2010, and there have been insufficient aircraft-based measurements over the BTH region, especially in recent years. Moreover, as a series of joint pollution prevention measures and action plans have been recently implemented, including the Air Pollution Prevention and Control Action Plan, there has been a confirmed improvement in the particulate matter (Zhang and Geng, 2019; Xiao et al., 2020); however, O_3 levels have increased, and worsening photochemical pollution has been observed (Li et al., 2019; Wang et al., 2016). O_3 is a critical photochemical pollutant due to its important influence on air quality, climate change and atmospheric chemistry; thus, it is necessary to determine how it affects atmospheric pollution.

In this study, in-situ field aircraft measurements were performed over the BTH region in the summer of 2016. Simultaneous measurements using both aircraft and tethered-balloon were also conducted for the first time on a selected day in Gaocun to study the influence of PBL on the vertical distributions of pollutants. The spatial and vertical distributions of SO_2, NO_x, CO and O_3 from 12 flights were investigated, and the impact of regional transport of these pollutants over the BTH region was analyzed. Overall, this study provides insight into the characteristics of gaseous pollutants in the lower troposphere, and the results may support future environmental assessment and regional transport models over the BTH region.

2. Methods

2.1. Observation and instrument information

From June 17th to July 22nd 2016, gaseous pollutants (SO_2, NO_x, CO and O_3) were measured by an aircraft (Harbin Yun-12 Twin Engine Turboprop Utility Aircraft, Harbin Aircraft Manufacturing Company) with a cruising speed of approximately 180 km·h^{-1}. 12 flights, with about 27 h of total flight time, were performed over four different flight routes, as shown in Fig. 1, and more detailed flight information is summarized in Table 1. The take-off and landing airport for each flight was Tianjin Binhai International Airport (BA in Fig. 1). The highest flight altitude was about 2400 m, which placed the aircraft in the free troposphere where the flight crew did not need oxygen masks (the aircraft was unpressurised). Note that the actual flight routes may have been slightly adjusted according to the weather conditions and air traffic control.

To better understand the influence of boundary layer development in the daytime, tethered balloon-based measurements were also carried out during the aircraft observation period in the rural site of Gaocun (G in Fig. 1), which is located in between Beijing and Tianjin. The surrounding areas are mainly villages and farmland, and there are no apparent industrial emission sources or large buildings. There is a national highway (G103) approximately 4 km northeast of the observation site and the Beijing-Tianjin expressway is located about 3 km away to the southwest of Gaocun. The tethered balloon platform has been described in our previous study (Li et al., 2015) and the monitoring instruments are shown in Table 2. Additionally, a ground air quality monitoring van and a ceilometer (Model: CL31, Vaisala, Finland) were set up in the observation field to detect air pollutants and determine the mixing layer height (MLH), respectively. In the early morning of June 17th, a spiral flight was conducted by the aircraft over the Gaocun site from 2400 m to 200 m in flight radius circles of about 4 km (4:56–5:27). At the same time, we performed a tethered balloon-based observation on June 17th, and the maximum altitude was about 900 m and the observation time was from 4:20 to 7:20. To the best of our knowledge, this is the first simultaneous implementation of large tethered balloon-based and aircraft-based measurements in the lower troposphere.

Ambient air was introduced into the aircraft cabin through the forward-facing stainless-steel cone-type isokinetic inlet. Several commercial instruments (Table 2) were linked to the isokinetic sampling device via a Teflon tube and then fixed in the aircraft cabin. The detailed operational principles of these instruments have been described by Zhang et al. (2014). Raw gaseous pollutant data were recorded every 5 s, and then data were processed, with the reprocessed data having a resolution of 1 min. In addition, meteorological parameters (temperature: T and relative humidity: RH) and geographical information (latitude,

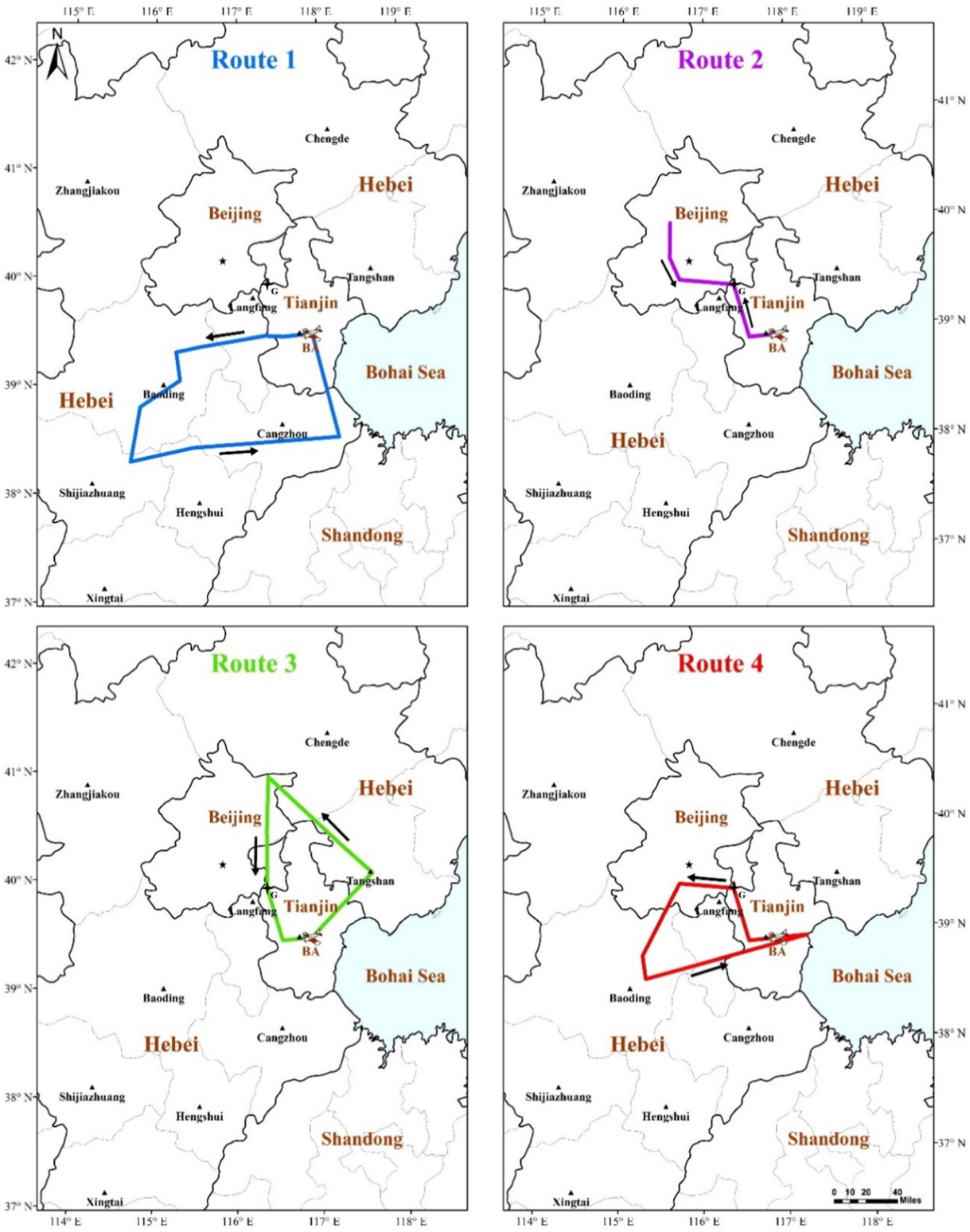

Fig. 1. Four flight routes during the aircraft sampling period. The small airplane model and cross symbol in the figure indicate the location of Tianjin Binhai International Airport (BA) and Gaocun (G), respectively. The corresponding flights for every route are: Route 1–July 3, July 13, July 18, July 22; Route 2–June 17, June 23; Route 3–June 19, July 17; Route 4–July 4, July 5, July 8, July 10.

longitude, and altitude) were measured by a cooling dew point meter (DewSTAR-1, Japan) with a resolution of 1 min and a global positioning system (GPS).

In order to guarantee the quality and reliability of the data, all instruments were examined thoroughly, and gas-tightness inspection was performed before every flight. Span calibrations were conducted before observations by injecting standard reference gas mixtures. Zero checks were made using a zero-air generator (TEI, model/111). An isokinetic inlet was mounted in front of the engines to avoid the impact of aircraft emissions and located at about 40 cm below the belly of the fuselage to keep it away from the blank and strengthening airstream areas due to the airflow through the airframe.

Table 1
Detail information for different flight routes.

Route	Date	Take off-landing (Beijing time)	Main altitude (m)	Total time (min)	Main area
1	July 3	4:53–7:18	600	145	Tianjin, Langfang, Baoding, Cangzhou
	July 13	17:13–20:09	1200, 1800	176	
	July 18	18:14–20:13	1500, 1800, 2400	119	
	July 22	18:50–20:51	2400	121	
2	June 17	4:27–6:15	600, 2400	108	Tianjin, Beijing
	June 23	5:09–6:40	600, 1200, 2400	130	
3	June 19	5:34–7:25	600, 1800	101	Tianjin, Tangshan, Beijing, Langfang
	July 17	11:15–13:16	1200, 1800	121	
4	July 4	14:02–16:23	600, 1200, 1500	141	Tianjin, Beijing, Baoding, Langfang
	July 5	4:49–7:05	1200	136	
	July 8	16:16–18:26	600, 1200	130	
	July 10	4:40–7:12	600, 1200	152	

2.2. Back trajectory analysis

The Hybrid Single-Particle Lagrangian Integrated Trajectory (HYSPLIT) model from the National Oceanic and Atmospheric Administration (NOAA) has been widely used to investigate the source regions and transport patterns of air pollutants in many aircraft-based measurements studies (Chen et al., 2013; Ding et al., 2008; Zhang et al., 2014; Wang et al., 2008; Li et al., 2012; Draxler, 1991). In this study, two-days backward trajectories were computed using the HYSPLIT model along the flight track. The parameters were set according to the exact altitude, time, and location of every aircraft flight. Meteorological data were from the Global Data Assimilation System (GDAS), which has a spatial resolution of $1° \times 1°$. The model vertical velocity and 12 h tagged temporal resolution were used to drive the model.

3. Results

3.1. Temporal and spatial variations of gaseous pollutants at different altitudes

Fig. 2 presents the concentrations of SO_2, NO_x, CO and O_3 for each flight at different altitudes. The aircraft routes covered a sizable horizontal area over the BTH region, so that the data could supply useful information on the spatial distributions of air pollutants. Figs. 3–6 show the spatial variations of SO_2, NO_x, CO and O_3 along the flight track at different altitudes. Relatively large horizontal variations were observed between different flights at 600 m, while the concentrations above 1500 m showed slight horizontal variation. High concentrations of primary pollutants (SO_2, NO_x, CO) generally appeared in Beijing, Tianjin, Langfang and Tangshan areas, while high values of O_3 frequently appeared in the areas far from the city, which agreed with the aircraft observations in the Yangtze River Delta region (Geng et al., 2009).

Overall, the SO_2 concentrations decreased with increasing altitude for each flight. NO_x presented similar variations with SO_2 in the morning flights; however, the flights at noon and dusk were different, with lower NO_x concentrations at 600 m than those at 1200 m on July 4th and 8th. CO has a long lifetime of about one month and is less reactive than SO_2 and NO_x; therefore, it can be transported by air masses over long distances and can accumulate in the lower troposphere. In this study, CO decreased with altitude in most flights (except for July 8th and 10th). The highest CO values were mainly observed at 600 m and 1200 m, and >1 ppm was also measured above 1500 m.

Compared with primary pollutants, the O_3 concentration showed different variations at different times of the day. In the morning flights, the O_3 concentrations increased with altitude except for June 19th, while the flights at noon and dusk all showed lower O_3 concentrations at higher altitudes. Higher O_3 values were also measured in the flights at noon and dusk. Echoing with the lower NO_x concentrations, the highest O_3 values were measured at 600 m on July 4th and 8th. Ozone is a secondary pollutant that is mainly produced by photochemical reactions in the lower troposphere, especially in summer. Although stratosphere-troposphere transport may contribute to tropospheric O_3 (Hocking et al., 2007), the results in this study indicated a major influence by photochemical sources over the BTH region.

3.2. Ground measurement on June 17th in Gaocun

Fig. 7 shows the diurnal variations of SO_2, NO_x, CO and O_3 from the ground monitoring van on June 17th in Gaocun (time in the figure is Beijing time). The mean concentrations of SO_2, CO, NO_2 and O_3 all met the Chinese Ambient Air Quality Standards (CAAQS, GB3095-2012) Grade II standards. SO_2 showed low concentrations and small changes throughout the day and the diurnal variation of NO_x showed a bimodal pattern. The SO_2, NO_x and CO concentrations all decreased between 10:00 and 13:00, while O_3 first increased, reached a maximum value at noon, and then declined significantly from 12:00 to 13:00. In addition, there was a sharp peak in O_3 at 22:00.

3.3. Simultaneous measurements from tethered balloon and aircraft on June 17th in Gaocun

Figs. 8 and 9 show the vertical distributions of SO_2, NO_x, CO and O_3 obtained from aircraft-spiraled and tethered balloon measurements on June 17th in Gaocun. In order to present the vertical variations clearly, the two-dimensional point-line figure was also plotted for aircraft-spiraled measurements (see supplemental material, Fig. S1). A notable "two-layer" vertical distribution with a dividing altitude of about 500 m was observed. Below 500 m, the pollutants were well mixed, and SO_2, NO_x, and CO showed relatively higher levels than those measured above 500 m; however, O_3 concentrations were lower below 500 m. The synchronous measurement results by tethered balloon revealed a similar distribution pattern, with relatively high SO_2, NO_x and CO concentrations and low O_3 concentrations below 500 m. The vertical distributions implied that the PBL height was about 500 m during the observation period in Gaocun, which was consistent with the ceilometer measurements (Fig. S2 in the supplemental material). Furthermore, an obvious high O_3 layer (79.9 ± 2.5 ppb) between 500 m and 1000 m was observed by aircraft and the tethered balloon also measured elevated O_3 values between 500 m and 900 m.

Table 2
Basic parameters of the observation instruments.

Methods	Species	Model	Technique	Range (ppm)	LDL (ppb)	Supplier
Aircraft	SO_2	43i-TLE	Pulsed ultraviolet fluorescence method	0–1	0.05	Thermo Fisher Scientific, USA
	NO_x	42i	Chemiluminescence method	0–0.5	0.40	
	CO	48i	Gas filter correlation method	0–10,000	0.04 ppm	
	O_3	49i	Double chamber ultraviolet photometry	0–0.5	0.5	
Tethered balloon	SO_2	AF 22M	Ultraviolet fluorescence method	0–0.5	0.4	Environnement S.A, France
	NO_x	AC 32M	Chemiluminescence method	0–0.5	0.4	
	CO	CO 12M	Gas filter correlation method	0–300	0.035 ppm	
	O_3	O_3 42M	Ultraviolet photometry	0–10	0.2	

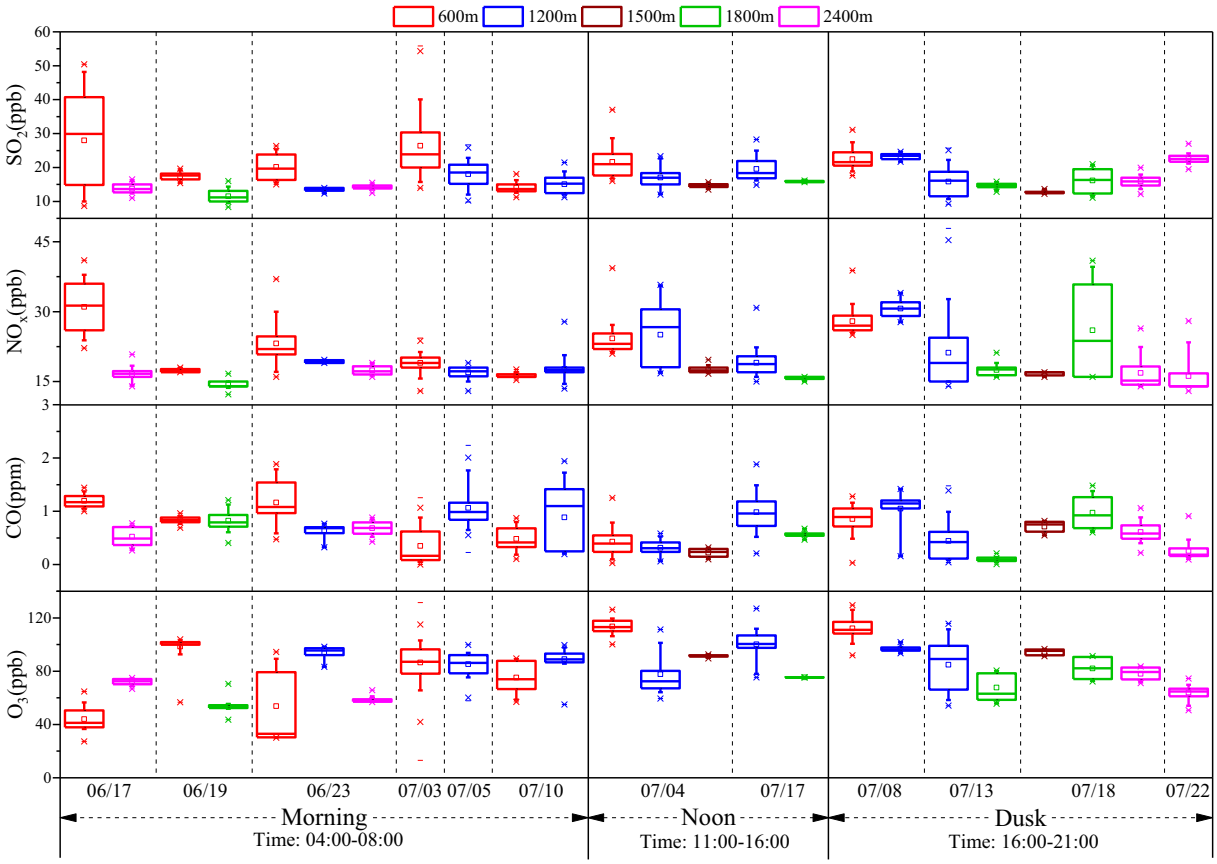

Fig. 2. Concentrations of SO_2, NO_x, CO and O_3 for each flight at different altitudes. The morning, noon, and dusk in the figure were classified according to the actual flight time; the corresponding time (Beijing time) are 4:00–8:00, 11:00–16:00, and 16:00–21:00 for morning, noon, and dusk, respectively. The upper and lower "—" markers are maximum and minimum values; the " × " markers above and below the whiskers represent the 99th and 1th percentiles; the whiskers above and below the boxes are the 90th and 10th percentiles; the upper and lower boundaries of the boxes indicate the 75th and 25th percentiles; the lines and the squares inside the boxes are the median and mean values.

4. Discussion

4.1. Comparison with some other aircraft measurements in China

Although many factors influence the concentrations of pollutants, e.g., meteorological conditions, observation period, sampling altitude, and local emission, a rough comparison with other studies is still useful to explore overall vertical distributions. Table 3 presents the observations of this study and other aircraft measurements across the world.

Compared with this study, CAREBeijing-2008 (Zhang et al., 2014) observed very low concentrations of gaseous pollutants, possibly due to the implementation of strict pollution control measures and the

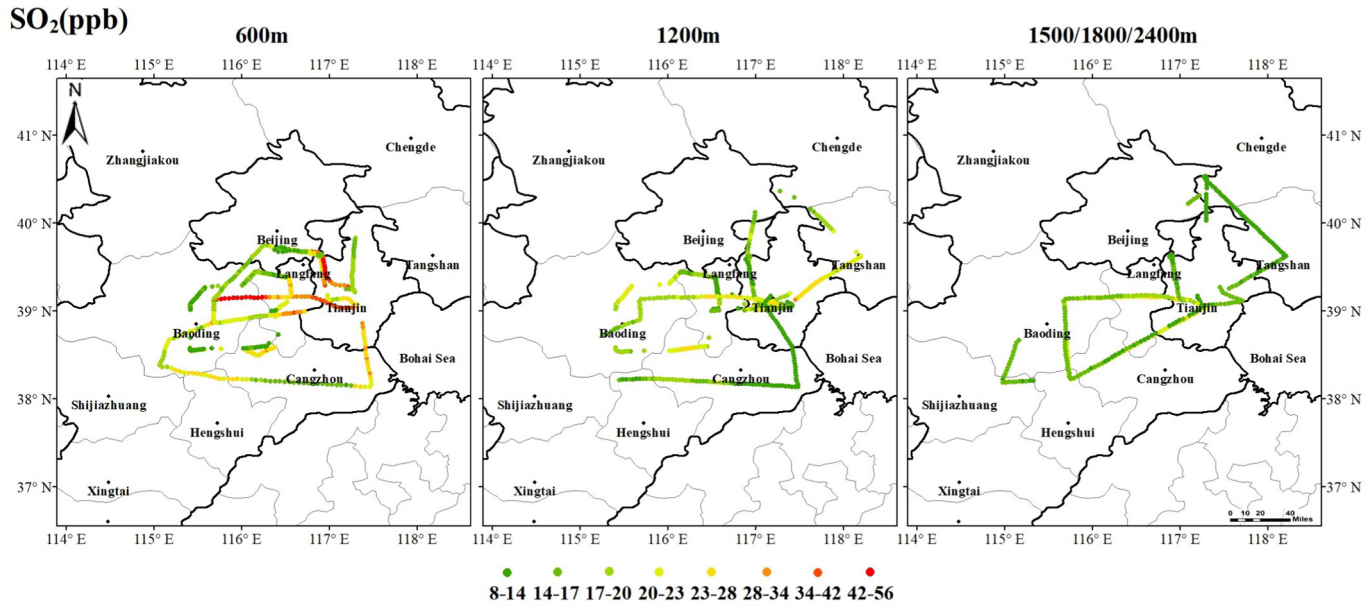

Fig. 3. Flight track of all data collected from the aircraft at different altitudes (600 m, 1200 m and above 1500 m) for SO_2 during the observation.

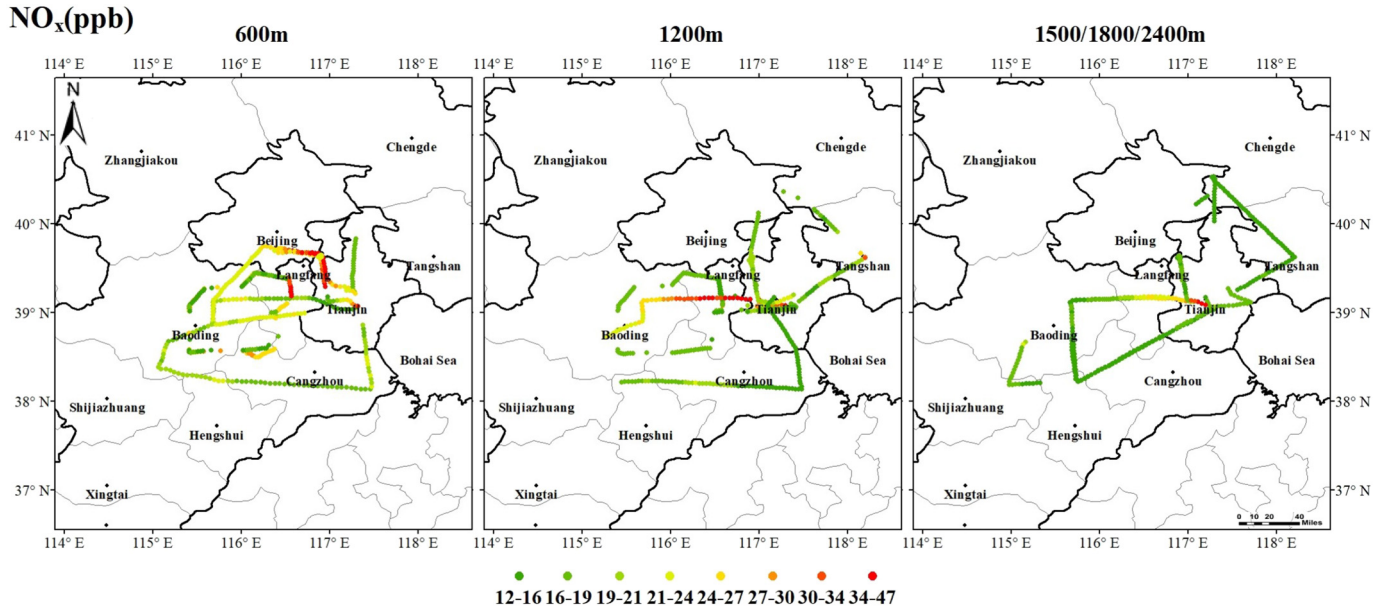

Fig. 4. Flight track of all data collected from the aircraft at different altitudes (600 m, 1200 m and above 1500 m) for NO_x during the observation.

favorable meteorological conditions during the Olympic Games. Compared with the results observed in April and May 2006 over the BTH region (Ma et al., 2012), this study showed significantly lower SO_2 concentrations and slightly higher NO_x concentrations. The lower SO_2 concentration could be attributed to the significant reduction in industrial SO_2 emissions due to the installation of flue-gas desulfurization devices in power plants and electrostatic precipitators in steel-making, iron-making, and cement production process (Li et al., 2017a). Vehicle emissions and industrial activities are major sources of NO_x in China. According to the China Statistical Yearbook (http://www.stats.gov.cn/tjsj/ndsj/), the number of private automobiles increased from 3.28 million in 2006 to 16.53 million in 2016 over the BTH region; however, low-NO_2 burner and denitrification technologies (SCR or SNCR) were widely installed after new emission standards were implemented, which considerably reduced NO_x emissions (Zheng et al., 2018). Therefore, the slightly higher NO_x concentrations were likely because the industrial NO_x emission reductions partly counteracted the increase in vehicle emissions. Additionally, the SO_2 and NO_x levels in this study were comparable to or higher than those observed in the Yangtze valley (Su, 2006). Compared with the aircraft measurements over Pearl River Delta (Wang et al., 2008), the SO_2 and NO_x levels in this study were slightly higher or comparable to those measured above 1500 m and were much lower than those measured at 600 m and 1200 m. The flight routes over the Pearl River Delta mainly deployed over the city in 'Circle' patterns; this meant that surface sources may have had more influence on the pollutants in the lower atmosphere.

The O_3 concentrations in this study were typically higher than those obtained in previous observations conducted over the BTH region (Ding et al., 2008; Ma et al., 2012; Zhang et al., 2014). Ding et al. (2008) studied the decadal trend of O_3 concentrations over Beijing and the North China Plain based on data from two periods (1995–1999 and 2000–2005) from the MOZAIC program. They observed an increase of

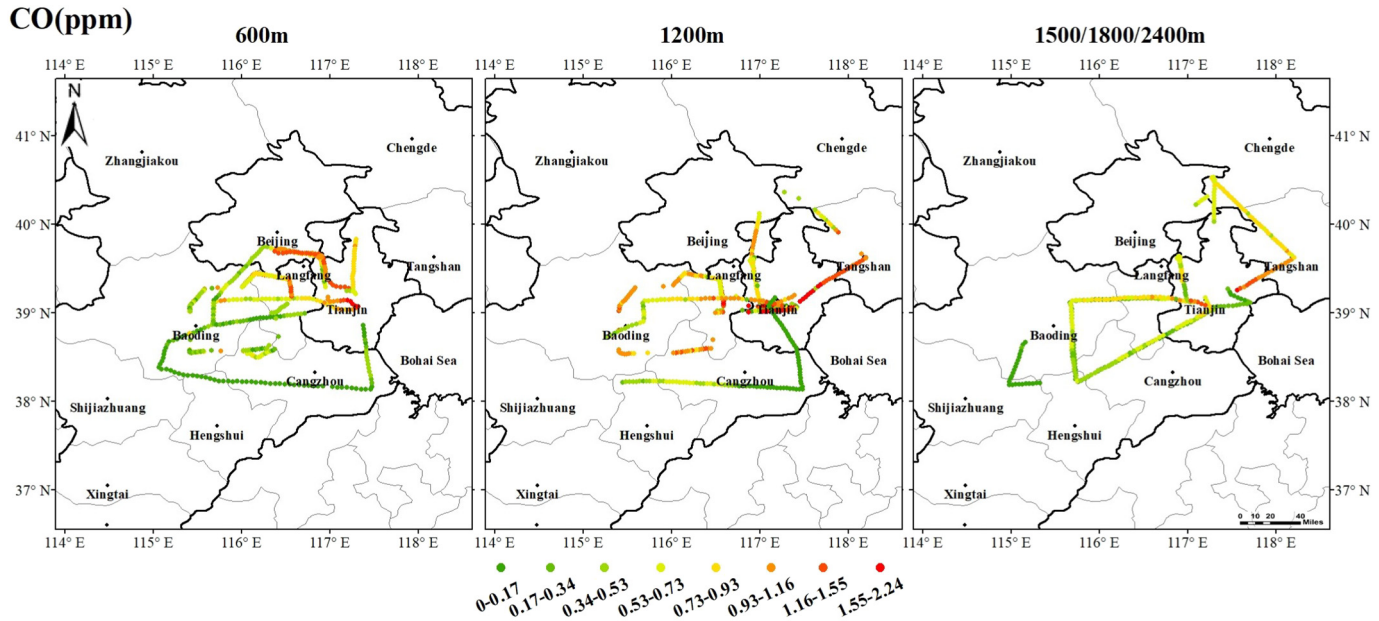

Fig. 5. Flight track of all data collected from the aircraft at different altitudes (600 m, 1200 m and above 1500 m) for CO during the observation.

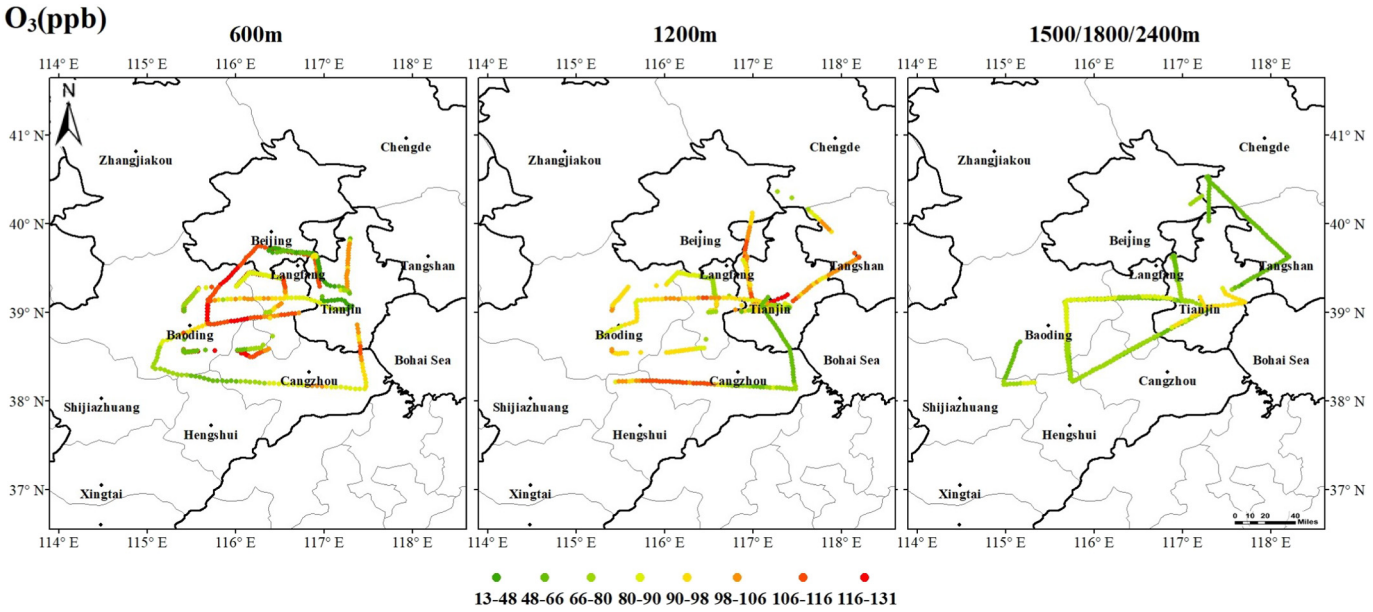

Fig. 6. Flight track of all data collected from the aircraft at different altitudes (600 m, 1200 m and above 1500 m) for O_3 during the observation.

approximately 2% per year, which may be related to increasing anthropogenic NO_x emissions. Surface ozone also increased (3.1 ppbv a^{-1}) for 2013–2017 over the BTH region (Li et al., 2019). In addition to NO_x, VOCs play an important role in photochemical reaction of O_3 formation. Vehicle emissions are another major contributor to NMVOCs in Beijing (Wang et al., 2014), and VOCs emissions are estimated to have significant increase in recent years (Zheng et al., 2018). The increase in VOCs emissions increased O_3 production. Moreover, the remarkable decrease in the PM concentration over the BTH region may have promoted O_3 formation by affecting solar radiation and slowing down the aerosol sink of hydroperoxy radicals (Li et al., 2019). In addition, the O_3 levels in this study were also higher than those observed over the Pearl River Delta (Wang et al., 2008). As mentioned above, higher NO_x concentrations were measured over the Pearl River Delta because of the observation area over the city; thus, the titration effect from the reaction of NO and O_3 could have resulted in the lower O_3 concentration (Xu et al., 2011). In addition, the results of some aircraft studies conducted in other countries were also listed in Table 3. It could be found that this study showed higher mean O_3 and CO concentrations than those observed in Korea, India, America, and Europe. This result indicated that the BTH region had severe photochemical pollution in the lower troposphere.

4.2. Influence of the planetary boundary layer

The vertical distributions of pollutants are influenced by their sources, as well as vertical mixing processes, which are closely related to the temporal evolution of PBL. Fig. 10 shows the vertical variations of RH, T and potential temperature (θ) from the aircraft-spiraled measurements on June 17th in Gaocun. An inversion layer was observed between 500 m and 600 m in which RH sharply decreased. Similar results were also obtained by the tethered balloon, as shown in Fig. 9. The changes in θ and RH were associated with the sharp change in the gaseous pollutant concentrations, indicating that vertical transport between the lower and upper layers was suppressed (Ma et al., 2011).

SO_2, NO_x, and CO are mainly from anthropogenic surface emissions and are thus constrained within the PBL, which gave rise to higher concentrations below 500 m. Since the observation time was in the early morning, there was little local photochemical production near the ground. Additionally, the O_3 titration reaction with elevated NO is very active during the night. As a result, O_3 presented significantly lower concentrations below 500 m. Note that the CO concentrations were still >1 ppm between 500 m and 1000 m; this was likely due to the characteristics of the long lifetime and non-reactivity of CO, which could allow its partial transport through the inversion layer and accumulation in the

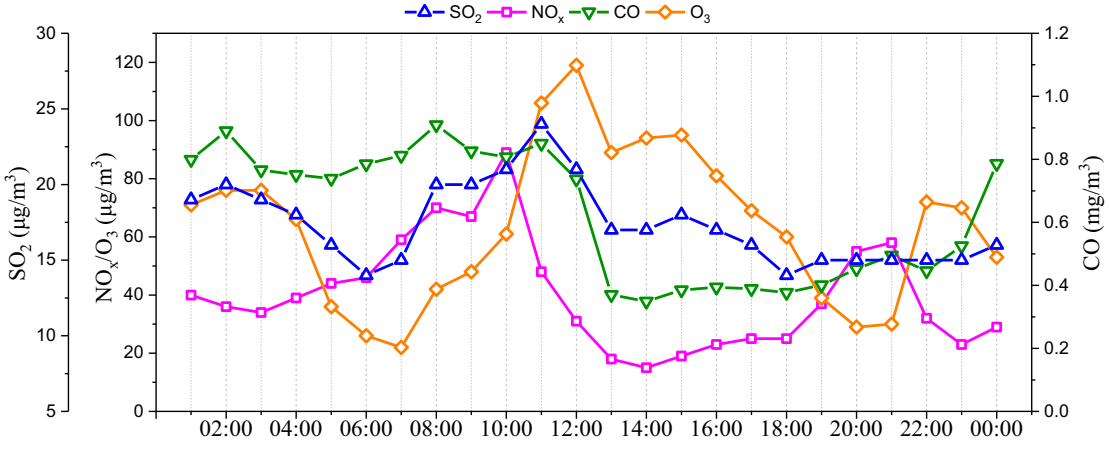

Fig. 7. The surface diurnal variations of SO_2, CO, NO_x, and O_3 concentrations on June 17th measured in Gaocun. Time in the figure is Beijing time.

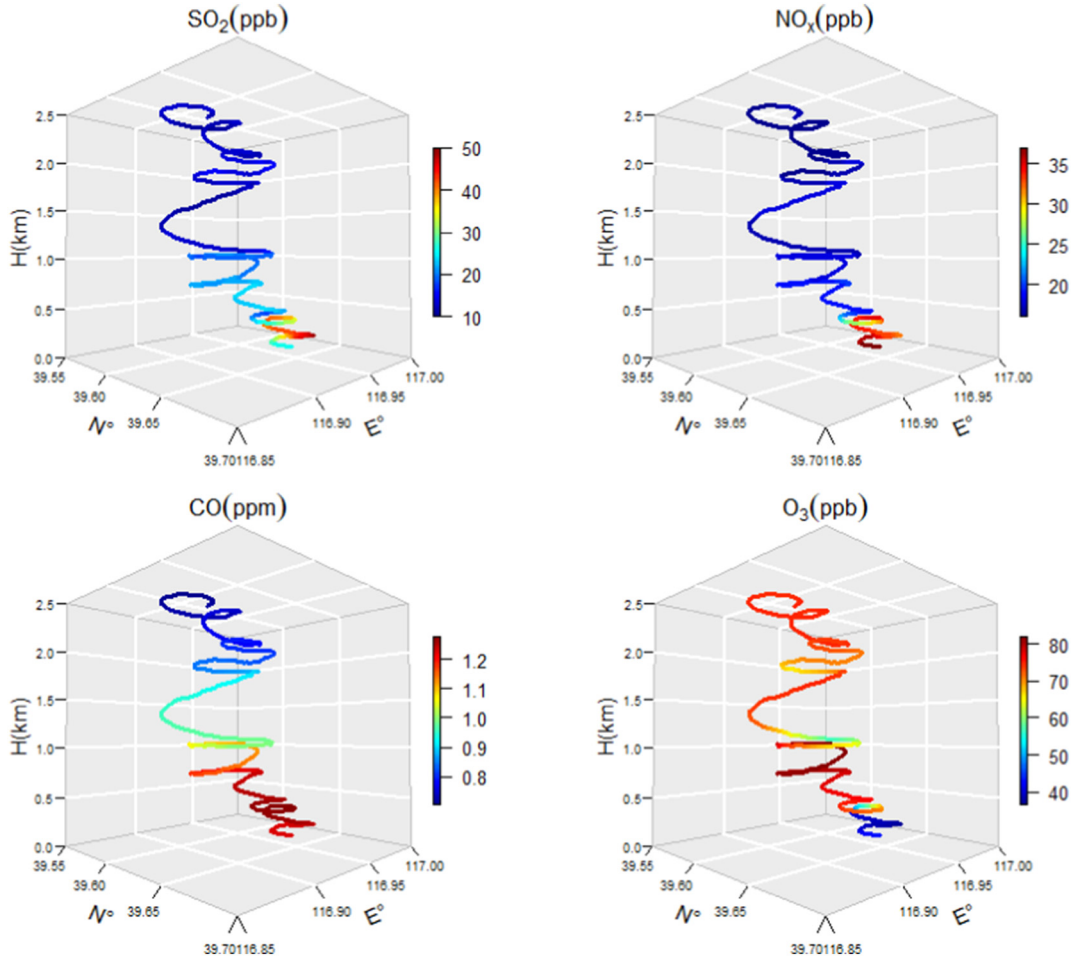

Fig. 8. Variations of SO_2, NO_x, CO and O_3 concentrations along the spiraled route from aircraft measurement on June 17th in Gaocun.

lower troposphere. The high O_3 layer (500 m–1000 m) observed by aircraft and tethered balloon (Figs. 8 and 9) is usually named the residual layer. O_3 in the residual layer was attributed to the accumulation and regional transport of ozone produced from the previous day (Aneja et al., 2000; Ma et al., 2011; Zhao et al., 2019). In addition, the correlation coefficients among the four gaseous pollutants (SO_2, NO_x, CO, O_3) from tethered balloon and aircraft-spiraled measurements on June 17th in Gaocun were also calculated (see supplemental material, Table S1). For the tethered balloon measurement, the significantly positive correlations among SO_2, NO_x, CO, and negative correlations between SO_2, NO_x, CO and O_3 were measured. For the aircraft measurement, the correlations among SO_2, NO_x, and CO were similar with the results of tethered balloon, however, O_3 showed no significant correlation with SO_2, NO_x, and CO. The spiral flight conducted by the aircraft over the Gaocun was from 2400 m to 200 m. Above the high O_3 residual layer (500 m–1000 m), the O_3 concentrations presented a sharp decrease from 1000 m to 1200 m, and then increased again above 1200 m, while the concentrations of SO_2, NO_x, and CO all showed decreased variation above 500 m (Figs. 8 and S1). Overall, the results of correlation analysis precisely supported the characteristics of vertical distribution.

The change of the PBL height may also influence the gaseous pollutants concentrations on the ground, and a negative correlation was observed between the PBL height and the concentrations of primary pollutants (He et al., 2017). As shown in Fig. S2 of the supplemental material, the PBL opened up rapidly at around 11:00 on June 17th in Gaocun, which produced enhanced vertical mixing and dispersion; therefore, the SO_2, NO_x and CO concentrations sharply decreased (Fig. 7). In contrast, the O_3 concentrations may have increased with the breakup of the PBL because O_3 in the residual layer was transported to the surface, thereby influencing the peak O_3 value (Aneja et al., 2000; Ma et al., 2011). In this study, the O_3 concentration first increased and then decreased between 11:00 and 13:00 (Fig. 7), which confirms this conclusion. Zhao et al. (2019) conducted the tethered balloon observations in Shijiazhuang (the capital city of Hebei province) in summer 2016 and concluded that O_3 in the residual layer in the morning accounted for 27% ± 7% of O_3 in the boundary layer at noon; thus, the influence of vertical transport on surface O_3 should be considered in future O_3 pollution control.

4.3. Impact of regional transport

In general, the diurnal variation of O_3 should display low O_3 levels after sunset because of the titration effect of NO and lower photochemical production; however, a sharp O_3 peak was measured at 22:00 on June 17th in Gaocun; therefore, another contributor to surface O_3 must exist. Intense vertical mixing was observed between 18:00 and 20:00, as illustrated in Fig. S2 of the supplemental material; therefore, we calculated the two-day backward trajectories at an altitude of 10 m AGL (above ground level) for arrival in Gaocun before (13:00–17:00) and after (20:00–24:00) the vertical mixing period (Fig. 11). The results showed that the air masses during the two periods arrived mainly from the northwest and first passed through Mongolia and Inner-Mongolia. Before arriving at Gaocun, the air masses at 13:00–17:00 reached a site due north of Gaocun and then turned directly south, while the air masses at 20:00–24:00 came from the west of Gaocun and passed south of the Beijing city area. Furthermore, the

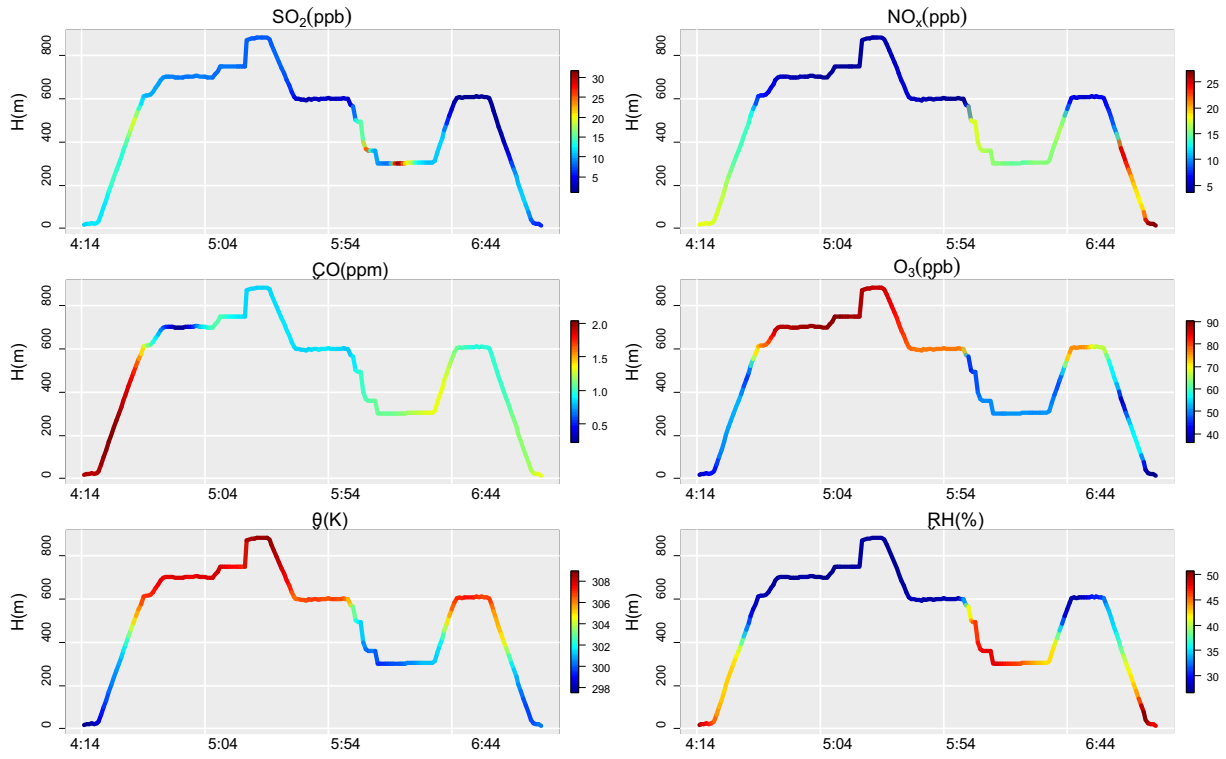

Fig. 9. Vertical variations of SO_2, NO_x, CO, O_3, potential temperature (θ) and relative humidity (RH) measured by tethered balloon on June 17th in Gaocun. Time in the figure is Beijing time.

air masses at 20:00–24:00 flowed at a greater altitude than those at 13:00–17:00 during transport. Thus, it was concluded that the convection process occurred and the wind direction shifted over two hours (18:00–20:00), and after this period, the air masses arriving at Gaocun contained more O_3, which increased the O_3 levels at 22:00–23:00.

Based on the origins and pathways of air masses determined in all flights, the trajectories were classified into three groups: from the south (G1), from the east and northeast (G2) and from the northwest (G3). The corresponding flights occurred on July 3rd, 4th, 8th, 10th, and 18th for G1; July 5th and 13th for G2; and, June 23rd and July 22nd for G3 (see supplemental material, Fig. S3). The air masses at different altitudes from the same flight could arrive from different directions, i.e., the air masses at 600 m on June 17th and 19th, and 1200 m on July 17th were from the south (G1), while the air masses at 2400 m on June 17th and 1800 m on June 19th and July 17th were from the northwest (G3). The SO_2, NO_x, CO, and O_3 results for G1–G3 are shown in the boxplots in Fig. 12.

The air mass trajectories in G1 had relatively short distances and low wind speeds and traveled across industrial and populated areas including Hebei, Shandong, and Henan Provinces. Therefore, this type of air mass could pick up more anthropogenic pollutants, which enabled pollutant accumulation in stagnant air before arriving at the sampling areas. During the observation period, air mass trajectories from more than 50% of the flights, especially at 600 m, belonged to G1, indicating that southerly transport has the greatest influence in the lower troposphere. As shown in Fig. 12, air masses in G1 contained higher concentrations than those in G2 or G3, in accordance with previous studies in the Beijing and Hebei regions (Ding et al., 2008; Zhang et al., 2014; Chi et al., 2018; Zhang et al., 2012). Independent T-tests were performed between the three groups for gaseous pollutants, T, and RH (Table 4). The results revealed significant differences between G1 and the other two groups, except CO between G1 and G2. Furthermore, exceptionally high concentrations of SO_2 and O_3 frequently occurred for G1, and G1 flows also circulated more air masses with higher T and RH.

The air mass trajectories in G2 suggested the possible impacts of the easterly and north-easterly flows, and there were only two days on all flights for G2. The concentrations of gaseous pollutants, especially NO_x and O_3, were found to lie between those of G1 and G3. Some extremely high values were also observed for NO_x and CO, which may be related to local surface emissions. G3 air masses had relatively long distances and high wind speeds, and the trajectories at 2400 m (except for those on July 18th) were all from G3. These types of air masses often contain lower levels of pollutants because of the fewer anthropogenic sources in the north-westerly regions. In this study, G3 generally displayed the lowest concentrations of gaseous pollutants, and the independent T-tests also showed a significant difference compared with the other groups, except SO_2 between G3 and G2. The results in this study were similar to those reported by Chi et al. (2018) and Zhang et al. (2014). Additionally, the lower T and RH of G3 also indicated a certain feature of the atmosphere from the mid-troposphere.

5. Conclusion

This study investigated the spatial and vertical distributions of SO_2, NO_x, CO, and O_3 over the BTH region using data obtained from 12 aircraft flights from June 17th to July 22nd, 2016. The results showed that the primary pollutants (SO_2, NO_x, CO) generally presented high concentrations in Beijing, Tianjin, Langfang and Tangshan areas, and high values of O_3 frequently appeared in the areas far away from the city. The flights at noon and dusk measured higher O_3 concentrations at 600 m and showed lower O_3 concentrations at higher altitudes, implying an important influence by photochemical production. The O_3 pollution levels were relatively severe in the lower troposphere, which was attributed to the increasing NO_x and VOCs emissions and the decrease of PM over the BTH region in recent years. During the observation period, transport by southerly air masses had the greatest influence on gaseous pollutants, especially at 600 m, and increased the concentrations of gaseous pollutants. In contrast, air masses from the

Table 3
Comparison of the trace gases at different altitudes in this study with other aircraft measurements across the world (the unit of CO is ppm, and the units of other gases are ppb).

Study area	SO_2	NO_x	CO	O_3	Time	Height (m)
BTH region	22.30	22.55	0.62	90.0	June–July 2016	600
	17.31	19.48	0.79	89.1		1200
	16.45	16.47	0.51	68.6		1500/1800/2400
BTH region[a]	8.79	15.41	0.52	64.47	August–October	600
	5.70	10.24	0.38	58.24	2008	900
	1.61	6.71	0.36	50.85		2100
BTH region[b]	~42	~20	~0.8	~42	April–May 2006	600
	~30	~18	~0.5	~43		1200
	26.2	10.6	0.23	41.2		1500–3000
Beijing and NCP[c]				~52	June–July	Surface-600
				~64	1995–2005	900–1500
				~62		2000–4000
Yangtze valley[d]	24	9		110	May–June 2004	600
	17	7		103		1000/1200
	6	2		85		1500/2100
Pearl River Delta[e]	48.46	52.82		61.66	October 2004	400–500
	40.70	43.85		63.77		700–800
	34.34	37.14		58.19		1000–1200
	16.86	8.08		43.10		2100 m
Tokyo, Japan[c]				~45	Annual mean,	600
				~47	2000–2005	1200
				~49		2000
Paris, France[c]				~35	Annual mean,	600
				~42	2000–2005	1200
				~49		2000
New York, America[c]				~40	Annual mean,	600
				~46	2000–2005	1200
				~50		2000
Delhi, India[f]			~0.18	~25	June–July	600
			~0.16	~38	2003–2005	1200
			~0.14	~40		2000
Washington, America[g]			0.169	47.9	April–May 2006	0–500
			0.155	50.4		500–1000
			0.139	60.6		1500–2500
South coastal region, Korea[h]			~0.358	~53.2	May–August	500
			~0.257	~54.8	2009	1000
			~0.274	~47.7		1500
South Regions of Western Siberia[i]				~60	July 2009	600
				~30		1200
				~23		2000

[a] (Zhang et al., 2014).
[b] (Ma et al., 2012).
[c] (Ding et al., 2008).
[d] (Su, 2006).
[e] (Wang et al., 2008).
[f] (Bhattacharjee et al., 2015).
[g] (Swartzendruber et al., 2008).
[h] (Seok et al., 2012).
[i] (Belan et al., 2011).

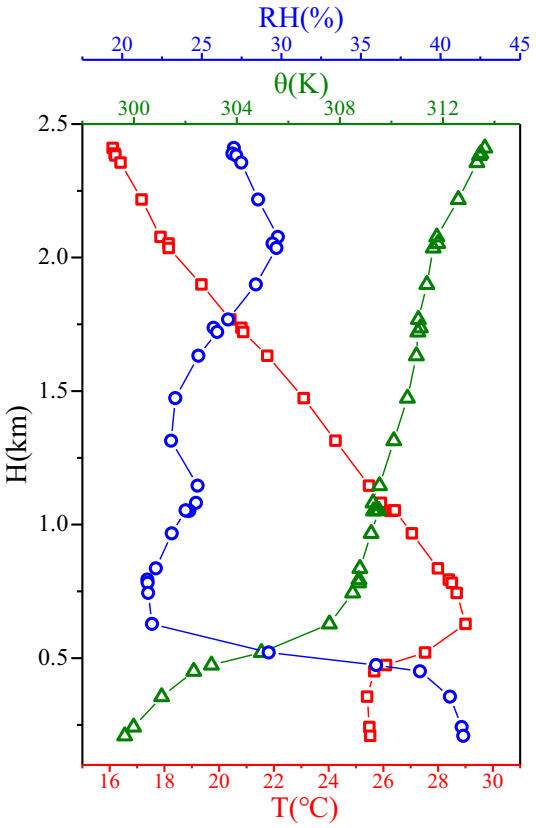

Fig. 10. Vertical variations of relative humidity (RH), temperature (T) and potential temperature (θ) obtained by aircraft-spiraled measurements on June 17th in Gaocun.

northwest typically delivered cleaner air, which was associated with lower concentrations of gaseous pollutants.

According to simultaneous measurements by aircraft and tethered balloon in Gaocun on June 17th, we observed a "two-layer" vertical distribution of gaseous pollutants above and below the PBL. This could be explained by the inversion layer at the top of the PBL, which significantly suppressed vertical exchange through the PBL. In addition, the high O_3 concentration observed in the residual layer—resulting from the accumulation and regional transport of ozone produced from the previous day—could increase the surface O_3 peak level at noon through downward transport along with the opening up of the PBL.

This study demonstrates the application potential of tethered balloon-based and aircraft-based measurements in the lower troposphere and provides basic data for calibrating future air quality and regional transport models. The findings of this study may increase the scientific understanding of the influence of PBL structure on the O_3 concentrations and imply that prevention and control measures should be performed in advance to mitigate predicted severe O_3 pollution. Furthermore, the results also indicate regional transport might play an important role under certain circumstances, and joint efforts are needed to reduce emissions over the whole BTH region. However, there are still some limitations to be improved in the future. For instance, the change of air pressure along with altitude during the flight should be considered in the subsequent study.

CRediT authorship contribution statement

Ruojie Zhao: Formal analysis, Methodology, Data curation, Sample collection, Investigation, Writing - original draft.
Baohui Yin: Sample collection.
Nan Zhang: Formal analysis, Methodology, Data curation.
Jing Wang: Methodology, Data curation, Resources.
Chunmei Geng: Methodology, Data curation, Sample collection, Writing - review & editing.
Xinhua Wang: Sample collection, Writing - review & editing.
Bin Han: Source, Conceptualization, Supervision, Writing - review & editing.
Kangwei Li: Writing - review & editing.
Peng Li: Sample collection.
Hao Yu: Writing - review & editing.
Wen Yang: Funding acquisition, Methodology, Investigation, Sample collection, Writing - review & editing.
Zhipeng Bai: Funding acquisition, Methodology, Writing - review & editing.

Declaration of competing interest

The authors declare that they have no known competing financial interests or personal relationships that could have appeared to influence the work reported in this paper.

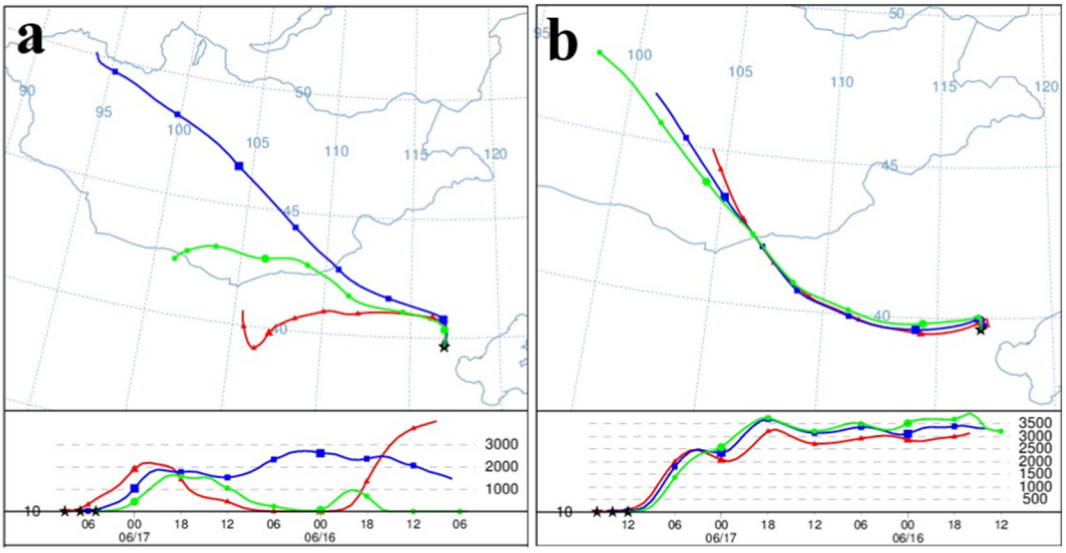

Fig. 11. The two-day backward trajectories arriving at Gaocun on June 17th and the arrival time (Beijing time) is 13:00–17:00 (a) and 20:00–24:00 (b). Time in the figure is UTC, which is 8 h later than Beijing time.

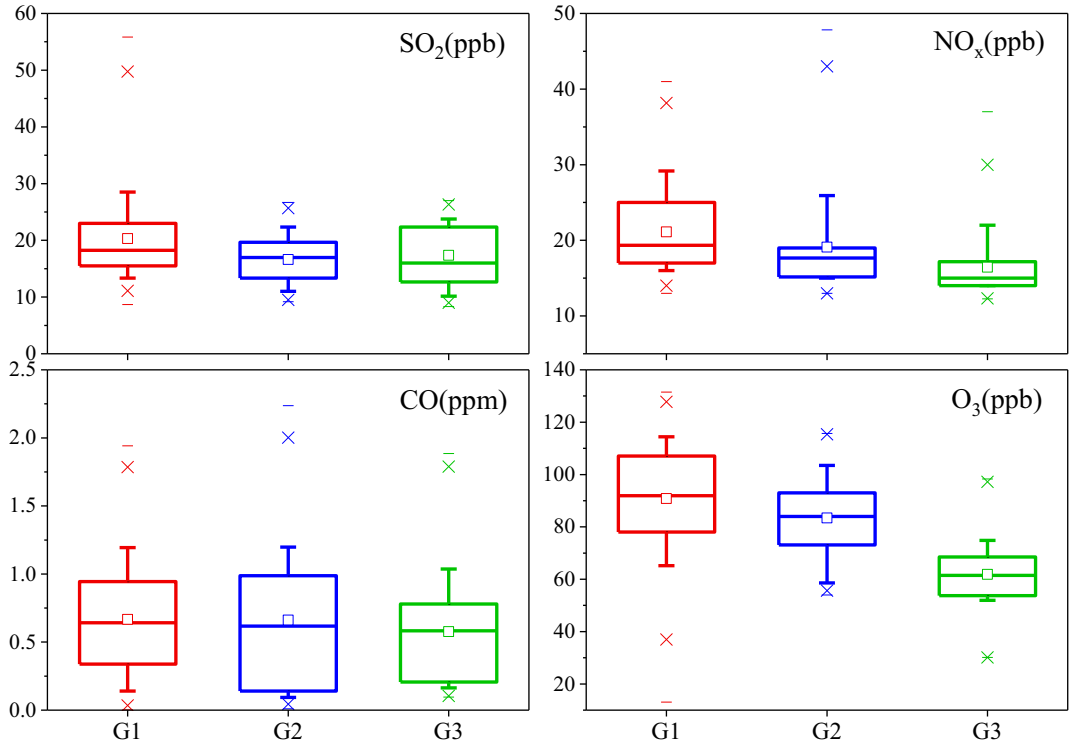

Fig. 12. Boxplots of SO_2, NO_x, CO and O_3 for three groups. The upper and lower "—" markers are maximum and minimum values; the " × " markers above and below the whiskers represent the 99th and 1th percentiles; the whiskers above and below the boxes are the 90th and 10th percentiles; the upper and lower boundaries of the boxes indicate the 75th and 25th percentiles; the lines and the squares inside the boxes are the median and mean values.

Table 4
The comparison of SO_2, NO_x, CO, O_3, T and RH values between the three groups (the unit of CO is ppm, and the units of other gases are ppb).

	Group 1			Group 2			Group 3			Independent T-test (*p* values)		
	Mean	SD	Median	Mean	SD	Median	Mean	SD	Median	G1–G2	G1–G3	G2–G3
SO_2	20.30	7.39	18.25	16.62	4.13	16.96	17.34	5.29	16.00	0.000	0.000	0.090
NO_x	21.11	5.66	19.33	19.10	5.85	17.67	16.44	3.78	15.00	0.000	0.000	0.000
CO	0.66	0.41	0.64	0.66	0.49	0.62	0.58	0.37	0.58	0.909	0.002	0.027
O_3	90.86	20.29	91.90	83.44	15.92	83.96	61.83	12.37	61.49	0.000	0.000	0.000
T(°C)	23.29	4.77	25.74	21.47	2.28	22.09	19.49	2.37	19.37	0.000	0.000	0.000
RH(%)	60.16	11.66	62.40	54.63	16.11	54.39	39.65	14.16	41.38	0.000	0.000	0.000

Acknowledgments

The authors gratefully thank the staff from Tianjin Environmental Monitoring Center, Zhongfei General Aviation Co., Ltd. and China Electronics Technology Group Corporation NO. 38 Research Institute for their technical support during the observations. This work was funded by the National Science and Technology Support Program (No. 2014BAC23B01) and National Key Scientific Instrument and Equipment Development Project (No. 2011YQ060111). We are also grateful to the NOAA Air Resources laboratory for the provision of the HYSPLIT transport and dispersion model used in this paper, and the anonymous reviewers for their critical comments and language editing.

Appendix A. Supplementary data

Supplementary data to this article can be found online at https://doi.org/10.1016/j.scitotenv.2020.144818.

References

Aneja, V.P., Mathur, R., Arya, S.P., Li, Y., Murray, G.C., Manuszak, T.L., 2000. Coupling the vertical distribution of ozone in the atmospheric boundary layer. Environ. Sci. Technol. 34, 2324–2329.

Belan, B.D., Tolmachev, G.N., Fofonov, A.V., 2011. Ozone vertical distribution in the troposphere over south regions of Western Siberia. Atmospheric Ocean. Opt. 24, 181–187. https://doi.org/10.1134/S1024856011020059.

Bhattacharjee, P.S., Singh, R.P., Nédélec, P., 2015. Vertical profiles of carbon monoxide and ozone from MOZAIC aircraft over Delhi, India during 2003–2005. Meteorog. Atmos. Phys. 127, 229–240.

Chang, X., Wang, S.X., Zhao, B., Xing, J., Liu, X.X., Wei, L., Song, Y., Wu, W.J., Cai, S.Y., Zheng, H.T., Ding, D., Zheng, M., 2019. Contributions of inter-city and regional transport to $PM_{2.5}$ concentrations in the Beijing-Tianjin-Hebei region and its implications on regional joint air pollution control. Sci. Total Environ. 660, 1191–1200.

Chen, P.F., Quan, J.N., Zhang, Q., Tie, X.X., Gao, Y., Li, X., Huang, M.Y., 2013. Measurements of vertical and horizontal distributions of ozone over Beijing from 2007 to 2010. Atmos. Environ. 74, 37–44.

Chen, Y., Zhao, C.S., Zhang, Q., Deng, Z.Z., Huang, M.Y., Ma, X.C., 2009. Aircraft study of mountain chimney effect of Beijing, China. J. Geophys. Res. Atmos. 114, 1–10.

Cheng, N., Li, Y., Cheng, B., Wang, X., Meng, F., Wang, Q., Qiu, Q., 2018. Comparisons of two serious air pollution episodes in winter and summer in Beijing. J. Environ. Sci. 69, 141–154.

Chi, X.Y., Cheng, L., Xie, Z.Q., Fan, G.Q., Yang, W., He, P.Z., Fan, S.D., Hong, Q.Q., Zhuang, W., Yu, X.W., 2018. Observations of ozone vertical profiles and corresponding precursors in the low troposphere in Beijing, China. Atmos. Res. 213, 224–235.

Ding, A.J., Wang, T., Thouret, V., Cammas, J.-P., Nédélec, P., 2008. Tropospheric ozone climatology over Beijing: analysis of aircraft data from the MOZAIC program. Atmos. Chem. Phys. 8, 1–13.

Draxler, R.R., 1991. The accuracy of trajectories during ANATEX calculated using dynamic model analyses versus rawinsonde observations. J. Appl. Meteorol. 30, 1446–1564.

Geng, F., Qiang, Z.X.T., Huang, M., Ma, X., Deng, Z., Yu, Q., Quan, J., Zhao, C., 2009. Aircraft measurements of O_3, NO_x, CO, VOCs, and SO_2 in the Yangtze River Delta region. Atmos. Environ. 43, 584–593.

Greenberg, J.P., Guenther, A.B., Turnipseed, A., 2009. Tethered balloon-based soundings of ozone, aerosols, and solar radiation near Mexico City during MIRAGE-MEX. Atmos. Environ. 43, 2672–2677.

Han, F., Xu, J., He, Y., Dang, H., Yang, X., Meng, F., 2016. Vertical structure of foggy haze over the Beijing–Tianjin–Hebei area in January 2013. Atmos. Environ. 139, 192–204.

He, J., Gong, S., Yu, Y., Yu, L., Wu, L., Mao, H., Song, C., Zhao, S., Liu, H., Li, X., 2017. Air pollution characteristics and their relation to meteorological conditions during 2014–2015 in major Chinese cities. Environ. Pollut. 223, 484–496.

He, J., Gong, S., Zhou, C., Lu, S., Wu, L., Chen, Y., Yu, Y., Zhao, S., Yu, L., Yin, C., 2018. Analyses of winter circulation types and their impacts on haze pollution in Beijing. Atmos. Environ. 192, 94–103.

Hocking, W.K., Carey-Smith, T., Tarasick, D.W., Argall, P.S., Strong, K., Rochon, Y., Zawadzki, I., Taylor, P.A., 2007. Detection of stratospheric ozone intrusions by windprofiler radars. Nature 450, 281–284.

Li, C., Stehr, J.W., Marufu, L.T., Li, Z., Dickerson, R.R., 2012. Aircraft measurements of SO_2 and aerosols over northeastern China: vertical profiles and the influence of weather on air quality. Atmos. Environ. 62, 492–501.

Li, J., Fu, Q., Huo, J., Wang, D., Yang, W., Bian, Q., Duan, Y., Zhang, Y., Pan, J., Lin, Y., Huang, K., Bai, Z., Wang, S.-H., Fu, J.S., Louie, P.K.K., 2015. Tethered balloon-based black carbon profiles within the lower troposphere of Shanghai in the 2013 East China smog. Atmos. Environ. 123, 327–338.

Li, K., Jacob, D.J., Liao, H., Shen, L., Zhang, Q., Bates, K.H., 2019. Anthropogenic drivers of 2013–2017 trends in summer surface ozone in China. Proc. Natl. Acad. Sci. 116, 422–427.

Li, R., Cui, L., Li, J., An, Z., Fu, H., Yu, W., Zhang, L., Kong, L., Chen, J., 2017a. Spatial and temporal variation of particulate matter and gaseous pollutants in China during 2014–2016. Atmos. Environ. 161, 235–246.

Li, X.B., Wang, D.S., Lu, Q.C., Peng, Z.R., Lu, S.J., Li, B., Li, C., 2017b. Three-dimensional investigation of ozone pollution in the lower troposphere using an unmanned aerial vehicle platform. Environ. Pollut. 224, 107–116.

Li, X.B., Wang, D.S., Lu, Q.C., Peng, Z.R., Wang, Z.Y., 2018. Investigating vertical distribution patterns of lower tropospheric $PM_{2.5}$ using unmanned aerial vehicle measurements. Atmos. Environ. 173, 62–71.

Liu, Q., Ding, D., Huang, M., Tian, P., Zhao, D., Wang, F., Li, X., Bi, K., Sheng, J., Zhou, W., Liu, D., Huang, R., Zhao, C., 2018. A study of elevated pollution layer over the North China Plain using aircraft measurements. Atmos. Environ. 190, 188–194.

Ma, J., Chen, Y., Wang, W., Yan, P., Liu, H., Yang, S., Hu, Z., Lelieveld, J., 2010. Strong air pollution causes widespread haze-clouds over China. J. Geophys. Res. 115, D18204. https://doi.org/10.1029/2009JD013065.

Ma, J.Z., Wang, W., Chen, Y., Liu, H.J., Yan, P., Ding, G.A., Wang, M.L., Sun, J., Lelieveld, J., 2012. The IPAC-NC field campaign: a pollution and oxidization pool in the lower atmosphere over Huabei, China. Atmos. Chem. Phys. 12, 3883–3908.

Ma, Z., Zhang, X., Xu, J., Zhao, X., Meng, W., 2011. Characteristics of ozone vertical profile observed in the boundary layer around Beijing in autumn. J. Environ. Sci. 23, 1316–1324.

Meng, Z.Y., Ding, G.A., Xu, X.B., Xu, X.D., Yu, H.Q., Wang, S.F., 2008. Vertical distributions of SO_2 and NO_2 in the lower atmosphere in Beijing urban areas, China. Sci. Total Environ. 390, 456–465.

Peng, Z.R., Wang, D., Wang, Z., Gao, Y., Lu, S., 2015. A study of vertical distribution patterns of $PM_{2.5}$ concentrations based on ambient monitoring with unmanned aerial vehicles: a case in Hangzhou, China. Atmos. Environ. 123, 357–369.

Quan, J., Jia, X., 2020. Review of aircraft measurements over China: aerosol, atmospheric photochemistry, and cloud. Atmos. Res. 243, 104972.

Sangiorgi, G., Ferrero, L., Perrone, M.G., Bolzacchini, E., Duane, M., Larsen, B.R., 2011. Vertical distribution of hydrocarbons in the low troposphere below and above the mixing height: tethered balloon measurements in Milan, Italy. Environ. Pollut. 159, 3545–3552.

Seok, S.J., Kim, S.Y., Lee, M.D., Choi, J.S., Kim, S.Y., Lee, S.J., Kim, J.S., Lee, G.W., 2012. The analysis of spatial distribution of ozone in the southern coast of Korea using the aircraft (2009, summer). J. Korean Soc. Atmos. Environ. 28 (1), 12–21. https://doi.org/10.5572/KOSAE.2012.28.1.012.

Shi, H., Critto, A., Torresan, S., Gao, Q., 2018. The temporal and spatial distribution characteristics of air pollution index and meteorological elements in Beijing, Tianjin, and Shijiazhuang, China. Integr. Environ. Assess. Manag. 14, 710–721.

Song, C., Lin, W., Xie, Y., He, J., Xi, C., Wang, T., Lin, Y., Jin, T., Wang, A., Yan, L., 2017. Air pollution in China: status and spatiotemporal variations. Environ. Pollut. 227, 334–347.

Su, H., 2006. Aircraft Measurement of Air Pollutants Over the Typical Regions of the Yangtze Valley. Chinese Research Academy of Environmental Sciences, Beijing, China (in Chinese).

Sun, Y., Song, T., Tang, G., Wang, Y., 2013. The vertical distribution of $PM_{2.5}$ and boundary-layer structure during summer haze in Beijing. Atmos. Environ. 74, 413–421.

Swartzendruber, P.C., Chand, D., Jaffe, D.A., Smith, J., Reidmiller, D., Gratz, L., Keeler, J., Strode, S., Jaegle, L., Talbot, R., 2008. Vertical distribution of mercury, CO, ozone, and aerosol scattering coefficient in the Pacific Northwest during the spring 2006 INTEX-B campaign. J. Geophys. Res. 113, D10305. https://doi.org/10.1029/2007JD009579.

Taubman, B.F., Hains, J.C., Thompson, A.M., Marufu, L.T., Doddridge, B.G., Stehr, J.W., Piety, C.A., Dickerson, R.R., 2006. Aircraft vertical profiles of trace gas and aerosol pollution over the mid-Atlantic United States: Statistics and meteorological cluster analysis. J. Geophys. Res. 111, D10S07. https://doi.org/10.1029/2005JD006196.

Tian, Y., Jiang, Y., Liu, Q., Xu, D., Zhao, S., He, L., Liu, H., Xu, H., 2019. Temporal and spatial trends in air quality in Beijing. Landsc. Urban Plan. 185, 35–43.

Villa, T.F., Gonzalez, F., Miljievic, B., Ristovski, Z.D., Morawska, L., 2016. An overview of small unmanned aerial vehicles for air quality measurements: present applications and future prospectives. Sensors. 16, 1072. https://doi.org/10.3390/s16071072.

Wang, M., Shao, M., Chen, W., Yuan, B., Lu, S., Zhang, Q., Zeng, L., Wang, Q., 2014. A temporally and spatially resolved validation of emission inventories by measurements of ambient volatile organic compounds in Beijing, China. Atmos. Chem. Phys. 14, 5871–5891.

Wang, T., Xue, L.K., Brimblecombe, P., Lam, Y.F., Li, L., Zhang, L., 2016. Ozone pollution in China: a review of concentrations, meteorological influences, chemical precursors, and effects. Sci. Total Environ. https://doi.org/10.1016/j.scitotenv.2016.10.081.

Wang, W., Ren, L., Zhang, Y., Chen, J., Liu, H., Bao, L., Fan, S., Tang, D., 2008. Aircraft measurements of gaseous pollutants and particulate matter over Pearl River Delta in China. Atmos. Environ. 42, 6187–6202.

Xiao, C.C., Chang, M., Guo, P.K., Gu, M.F., Li, Y., 2020. Analysis of air quality characteristics of Beijing–Tianjin–Hebei and its surrounding air pollution transport channel cities in China. J. Environ. Sci. 87, 213–227. https://doi.org/10.1016/j.jes.2019.05.024.

Xu, H., Xiao, Z., Chen, K., Tang, M., Zheng, N., Li, P., Yang, N., Yang, W., Deng, X., 2019. Spatial and temporal distribution, chemical characteristics, and sources of ambient particulate matter in the Beijing-Tianjin-Hebei region. Sci. Total Environ. 658, 280–293.

Xu, J., Ma, J.Z., Zhang, X.L., Xu, X.B., Xu, X.F., Lin, W.L., Wang, Y., Meng, W., Ma, Z.Q., 2011. Measurements of ozone and its precursors in Beijing during summertime: impact of urban plumes on ozone pollution in downwind rural areas. Atmos. Chem. Phys. 11, 12241–12252.

You, L., Liu, Y., 1995. Some microphysical characteristics of cloud and precipitation over China. Atmos. Res. 35, 271–281. https://doi.org/10.1016/0169-8095(94)00023-7.

Zhang, J.P., Zhu, T., Zhang, Q.H., Li, C.C., Shu, H.L., Ying, Y., Dai, Z.P., Wang, X., Liu, X.Y., Liang, A.M., Shen, H.X., Yi, B.Q., 2012. The impact of circulation patterns on regional transport pathways and air quality over Beijing and its surroundings. Atmos. Chem. Phys. 12, 5031–5053.

Zhang, K., Wang, D., Bian, Q., Duan, Y., Zhao, M., Fei, D., Xiu, G., Fu, Q., 2017. Tethered balloon-based particle number concentration, and size distribution vertical profiles within the lower troposphere of Shanghai. Atmos. Environ. 154, 141–150.

Zhang, K., Zhou, L., Fu, Q., Yan, L., Bian, Q., Wang, D., Xiu, G., 2019. Vertical distribution of ozone over Shanghai during late spring: a balloon-borne observation. Atmos. Environ. 208, 48–60.

Zhang, Q., Geng, G., 2019. Impact of clean air action on $PM_{2.5}$ pollution in China. Sci. China Earth Sci. 62, 1845–1846. https://doi.org/10.1007/s11430-019-9531-4.

Zhang, W., Zhu, T., Yang, W., Bai, Z., Sun, Y.L., Xu, Y., Yin, B., Zhao, X., 2014. Airborne measurements of gas and particle pollutants during CAREBeijing-2008. Atmos. Chem. Phys. 14, 301–316.

Zhang, Y.F., Xu, H., Tian, Y.Z., Shi, G.L., Zeng, F., Wu, J.H., Zhang, X.Y., Li, X., Zhu, T., Feng, Y.C., 2011. The study on vertical variability of PM10 and the possible sources on a 220 m tower, in Tianjin, China. Atmos. Environ. 45, 6133–6140.

Zhao, W., Tang, G.Q., Yu, H., Yang, Y., Wang, Y.H., Wang, L.L., An, J.L., Gao, W.K., Hu, B., Cheng, M.T., An, X.Q., Li, X., Wang, Y.S., 2019. Evolution of boundary layer ozone in Shijiazhuang, a suburban site on the North China Plain. J. Environ. Sci. 83, 152–160.

Zheng, B., Tong, D., Li, M., Liu, F., Hong, C., Geng, G., Li, H., Li, X., Peng, L., Qi, J., Yan, L., Zhang, Y., Zhao, H., Zheng, Y., He, K., Zhang, Q., 2018. Trends in China's anthropogenic emissions since 2010 as the consequence of clean air actions. Atmos. Chem. Phys. 18, 14095–14111.